RSC Sustainability

ROYAL SOCIETY OF CHEMISTRY

PAPER

View Article Online
View Journal | View Issue

Cite this: *RSC Sustainability*, 2025, **3**, 1397

The best of both worlds: stacked catalytic layers for the electrocatalytic generation of CO in zero-gap electrolysers†

Lucas Hoof,‡[a] Kevinjeorjios Pellumbi,‡[a] Didem Cansu Güney,[b] Dennis Blaudszun,[a] Franz Bommas,[a] Daniel Siegmund,[ac] Kai junge Puring,[a] Rui Cao,[d] Katharina Weber*[b] and Ulf-Peter Apfel*[ad]

Tailoring the properties of the catalytic layer (CL) and its architecture is crucial for enhancing both the efficiency and selectivity of CO_2 electrolysers. Traditionally, CLs for CO_2 reduction comprise of a single binder material or a combination that handles both ion conductance and the maintenance of a hydrophobic environment. In this work, we decouple these processes into two individual, stacked catalyst-containing layers. Specifically, a hydrophobic catalytic layer is placed on the gas diffusion layer to improve water management within the CL during CO_2R in zero-gap electrolysers. Additionally, a second catalytic layer, bound by an ion-conducting binder, facilitates the conduction of OH^- and HCO_3^-/CO_3^{2-} during CO_2R, thereby enhancing both ionic conductivity between the GDE and anion exchange membrane (AEM), as well as mechanical adhesion between different interfaces. Notably, we present a comprehensive stepwise optimization pathway for the CL, addressing both single and stacked CLs for CO_2-to-CO conversion at current densities of 300 mA cm^{-2}.

Received 8th August 2024
Accepted 3rd February 2025

DOI: 10.1039/d4su00453a

rsc.li/rscsus

Sustainability spotlight

Achieving a carbon-neutral society requires significant advancements in CO_2 electrolysis, especially for closing the carbon loop in industrial processes. Traditionally, low-temperature CO2 electrolysis suffers from inefficiencies and poor selectivity due to the reliance on single-material catalytic layers that must simultaneously manage ion conductance and hydrophobicity. These issues are particularly challenging at high current densities, where precise control over water management and ion transport is essential. Our research introduces a dual-layer catalytic architecture that decouples hydrophobic and ion-conducting functions. A hydrophobic catalytic layer on the gas diffusion layer tailors water management, while a second ion-conducting binder layer optimizes ion transport between the gas diffusion electrode and the anion exchange membrane. This design significantly improves CO_2-to-CO conversion efficiency and selectivity. Our study underscores the importance of ink engineering and rheological measurements in the development of catalytic layers, offering a foundation for creating long-term stable and more efficient CO_2R electrolysers. Our work supports UN Sustainable Development Goals (SDGs), including affordable and clean energy (SDG 7), industry, innovation, and infrastructure (SDG 9), and climate action (SDG 13).

Introduction

In the current energy transition to more sustainable production pathways, the electrolytic conversion of CO_2 (CO_2R) presents a highly interesting route, generating carbon-building blocks, such as CO, HCOOH, C_2H_4 among others.[1] Currently, the production of CO, and in some cases of syngas (CO/H_2 mixtures) holds the largest promise towards large-scale implementation and direct coupling with the already established Fischer–Tropsch process.[2] Specifically in the case of low-temperature CO_2 electrolysis, Ag-coated gas diffusion electrodes (GDEs) constitute the state-of-the-art cathodes for the generation of CO/syngas with zero-gap electrolysers (ZGEs) being the most efficient and load flexible reactor architecture for the generation of gaseous products, such as CO in a scalable and energy-efficient manner.[3]

Overall, within the field of CO_2 electrolysis, control of the reactive micro-environment has become a crucial point in recent years towards controlling the selectivity of CO_2R-electrolysers and maintaining stable catalytic performance to ensure industrial applicability.[4] One of the most employed approaches here involves the variation of the binder type and content in the cathode catalyst layer.[5,6] Specifically, catalytic

[a]*Fraunhofer Institute for Environmental, Safety and Energy Technology, UMSICHT, Oberhausen, Germany. E-mail: ulf-peter.apfel@umsicht.fraunhofer.de*

[b]*Aalen University, Research Institute for Innovative Surfaces FINO, Aalen, Germany. E-mail: katharina.weber@hs-aalen.de*

[c]*Inorganic Chemistry, Faculty of Chemistry and Biochemistry, Ruhr University Bochum, Bochum, Germany. E-mail: ulf.apfel@rub.de*

[d]*Key Laboratory of Applied Surface and Colloid Chemistry, Shaanxi Normal University, Xi'an, China. E-mail: ruicao@snnu.edu.cn*

† Electronic supplementary information (ESI) available. See DOI: https://doi.org/10.1039/d4su00453a

‡ These authors contributed equally.

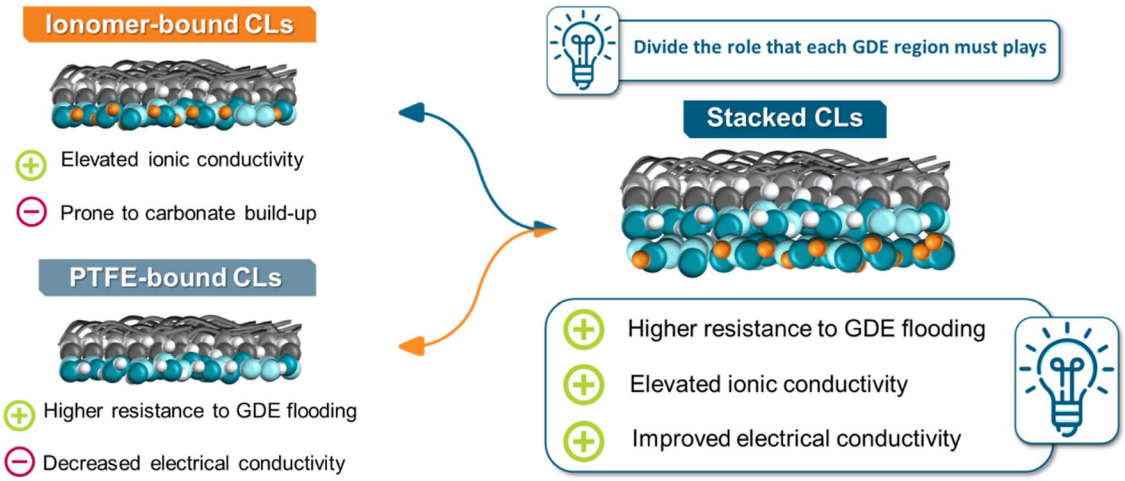

Fig. 1 Scheme overview of the novel catalytic layers generated within this investigation, with their associated advantages and disadvantages.

layers (CLs) in the field of CO_2 electrolysis can be separated into two major categories: (i) ionomer-bound ones and (ii) PTFE-bound ones. Ionomer-bound catalytic layers, employing often anion-exchange ionomers, allow the creation of an alkaline environment close to the catalytic centres, favouring CO_2R, while also "freeing" catalytic centres from reactive anionic species during electrolysis.[7] Nevertheless, ionomer-bound CLs are often prone to carbonate built-up within the pores of the GDE, through unintended cation crossover from the anolyte.[8] On the other hand, PTFE-bound CLs aim to favour CO_2R by introducing a hydrophobic environment close to the active centres and thus controlling the amount of water at the catalytic centres, though comes at the cost of ionic and electrical conductivity within the whole CL.[5,9]

Evidently, decoupling the different processes in ZGEs involving gas and ion-transport as well as balancing the CO_2 and H_2O concentration near the catalytic centres is difficult to achieve with GDEs employing only one type of binder.[5,10]

Moreover, as CO_2 electrolysis is transitioning to higher TRL levels it is necessary to effectively link catalyst ink characterization methods to the prediction of the final morphology of a CL and in hindsight its properties, prior to performing material and time intensive electrochemical characterisations of these CLs.[11,12] Reciprocally, this development pathway should accelerate the feedback loop for the characterisation of novel GDEs in a cost-effective manner.

Here, we conceptualized a stacked catalytic layer for the CO_2 to CO conversion in AEM-separated ZGEs (Fig. 1). Our goal was to combine the advantages of the two different types of CLs for the CO_2R, while mitigating their respective disadvantages. Here, an ionomer bound Ag-CL is placed on top of a PTFE-bound Ag-CL on the GDE, possessing both elevated ionic-conductivity close to the membrane interface, while also maintaining a hydrophobic environment close to the GDL support at 300 mA cm^{-2}. Furthermore, we provide the community with a pathway on how rheological ink investigations can assist into predicting the CL morphology, alongside a complete characterization scheme on how we identified the optimal CL compositions for the binder types. Our work underlines significant guidelines on how microscopical and rheological ink investigations can possibly become activity-predictors for CO_2R-focused investigation going beyond Ag-based electrodes.

Results and discussion

Rheology as a tool for predicting CL morphology

During a typical ultrasonic spray coating process, the ink is applied at room temperature, while the subsequent drying process takes place at 90 °C. In addition to the temperature differences between the two processes, there is a significant difference in the forces applied. High forces are applied during spray coating, whereas no forces are applied during the drying phase. To account for these contrasting conditions both processes and understand their effect on the rheological behaviour of the inks, storage and loss moduli were measured at temperatures of 25, 50 and 70 °C at a frequency range of 0.1 Hz to 100 Hz.

High frequencies simulate the rapid mechanical stress in the short-term range, *i.e.* the actual spraying process. Low frequencies, on the other hand, simulate the long-term or resting behaviour that should prevail before or after the spraying process. If the storage modulus G' (elastic component) is > than the loss modulus G'' (viscous component), solid structural behaviour is present; in the opposite case, the liquid character predominates. To determine the influence of the type of binder and the binder content, both PiperION-based and PTFE-based catalyser inks with binder contents of 1–30 wt% were investigated (Fig. 2 and S1†). These loading ranges were selected since at loadings below 1 wt% preliminary tests showed that the generated CLs, both for PiperION and PTFE suffer from significant mechanical instability, whilst at higher loading the deposition of the CL through spray-coating became less reliable and reproducible.

The PiperION-based catalyst ink has versatile rheological properties, which are mainly influenced by the binder content.

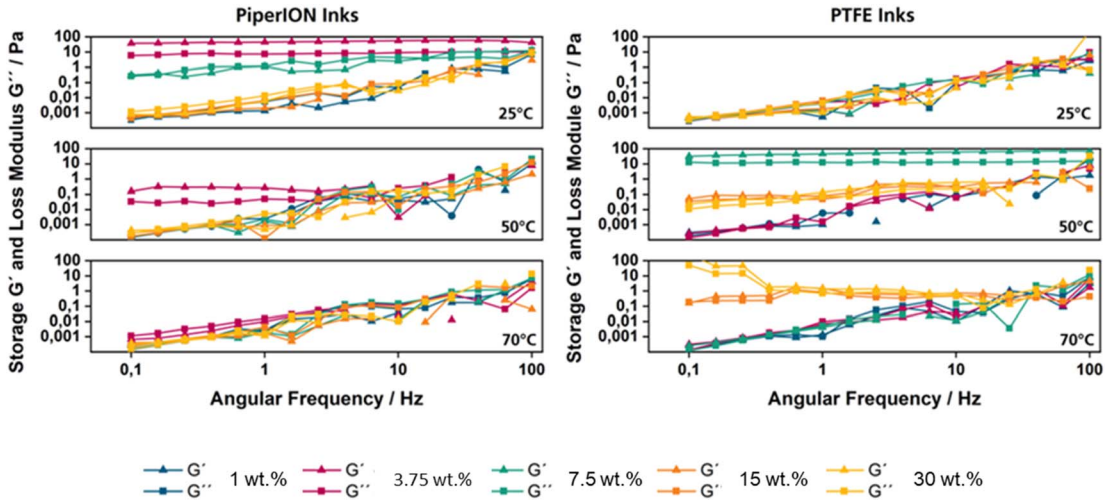

Fig. 2 Rheological characterization of the different employed inks by varying the temperature from 25 to 70 °C and the binder content from 1 to 30 wt%.

At a binder content of 3.75 wt%, it has a solid structure ($G' > G''$) at 25 °C with a structural strength of $G' = 48$ Pa. At 50 °C the PiperION ink remains solid below 10 Hz and transitions to a liquid state above this frequency, while at 70 °C it becomes completely liquid ($G'' > G'$). In other cases, especially at lower or higher binder contents, PiperION maintains a constant liquid structure at different temperatures (25 °C, 50 °C and 70 °C).

Similarly, the PTFE-based catalyst ink demonstrates a predominantly liquid structure ($G'' > G'$) across various temperatures and binder contents. Notably, at 50 °C, a binder content of 7.5 wt% induces a solid structure ($G' > G''$) with a strength of 53 Pa. At 70 °C, a binder content of 15 wt% transitions the ink to a solid state with a strength of 1.0 Pa, while at 30 wt% binder content, a dual behaviour is observed at 70 °C, with solid state below 25 Hz and a liquid state above 25 Hz. The rheological characteristics of the catalyst inks are also summarized in Table S1.†

In summary, both PiperION and PTFE catalytic inks generally exhibit liquid behaviour. Yet, PiperION undergoes a solid–liquid transition under certain conditions, while the PTFE-dispersions show a more solid behaviour under certain temperature and binder content combinations. These variations highlight sensitivity of these catalyst inks to specific processing conditions, with both exhibiting complex structural-viscous properties influenced by temperature and composition.

Crucially, the above predictions are mirrored in the obtained SEM analysis of the different CLs (Fig. S2 and 3†). Microscopic examinations of the PiperION-CL show highly porous structures at lower binder amounts (1–7.5 wt%) with the Ag-NPs becoming gradually engulfed in the solid ionomer matrix as the binder content is increased. Moreover, at higher PiperION amounts (>7.5 wt%) cracks in the CL structure are visible, possibly affecting the accumulation of water and salts precipitates during the CO_2R operation. Here, the dense CL-structure at higher PiperION amounts, alongside the infiltration of the flowable ionomer in the GDL pores, result in a declined mass transport, reflected in the low BET-surface area values (Table S2†). In contrast to the PiperION-based CLs, the PTFE-bound GDEs show a porous surface across all binder variations, attributable mainly to the lower flow behaviour of the PTFE ink, creating distinct ''islands'' of PTFE and Ag-NPs on the surface of the GDE. Notably, as the binder content is increased, this observation becomes more evident in the more rigid PTFE-structure, with distinct agglomerates of Ag-NPs and PTFE-particles emerging without these fully intermixing with each other (Fig. S3†). Furthermore, the employment of PTFE as the CL binder does not appear to change the BET surface area of the investigated GDEs (Table S2†).

Electrochemical investigation of the single catalytic layers

To set the basis for our stacked CLs and thus gain a complete understanding of the influence of the binder type and content on the physical and electrolytic properties the amount of the binder (1–30 wt% relative to the catalytic mass) was varied. While PiperION-bound GDEs could be directly employed for the CO_2R, PTFE-based ones require an intermediate annealing step to remove organic surfactants in the PTFE-dispersion and create a mechanically rigid structure.[6,13]

Electrochemical investigations were performed in our previously reported ZGE setup, placed within an oven at 60 °C being equipped with a temperature-controlled bubbler.[14] Here, parallel Ti-flow fields were employed to circulate the wetted CO_2 to the GDE as well as the 0.1 M $KHCO_3$ anolyte to the IrO_2 catalytic layer, performing electrolysis at 300 mA cm^{-2} for 3 hours of electrolysis. The discussion provided herein focuses on the results obtained between the 2nd and 3rd hour of electrolysis, as we believe this timeframe to accurately mirror a more stable performance region in the case of such characterization tests (Fig. S4†).[14]

Starting with the electrochemical characterization of the distinct catalytic layers, an interesting trend emerges between the different binders. The PiperION-bound CLs show the

highest value for the faradaic efficiency for CO (FE_{CO}) (49%) at the lowest binder content (1 wt%) demonstrating a continuous decrease of FE_{CO} with increasing binder content, down to 12% at 30 wt% (Fig. 3a). On the other hand, the PTFE-bound CL show a pyramid shaped trend, with the peak value for the FE_{CO} of 43% located at a medium binder content of 7.5 wt%. Regarding the cell voltages (U_{Cell}), PiperION-bound CLs show U_{cell} values between 3.0 – 3.2 V at 300 mA cm^{-2}, whereas values of the PTFE-bound counterpart range between 3.5 and 5.5 V (Fig. 3b). Moreover, in the case of the PTFE-based CLs, the U_{Cell} values continuously increase with an increasing amount of binder, with samples containing 30 wt% PTFE exceeding 4.0 V leading to a highly unstable electrolysis behaviour. EIS analysis of the HFR frequency also showed that with an increasing amount of binder the HFR of the respective MEA-assemblies increases (Fig. S5†). Since all other parameters were kept the same, we attribute this change to a rising electrical resistance in the different CLs.[15]

The obtained trends overall are in accordance with the predictions set by the rheological and SEM analysis. At higher ionomer contents the particles become engulfed by the ionomer due to their higher flow behaviour in the ink composition, limiting access of CO_2 to the active centres.[12,15] On the other hand, increasing the PTFE-content within the ink, possibly also limits the proper wetting of the catalytic particles during electrolysis. Proper control of relative humidification in the CO_2

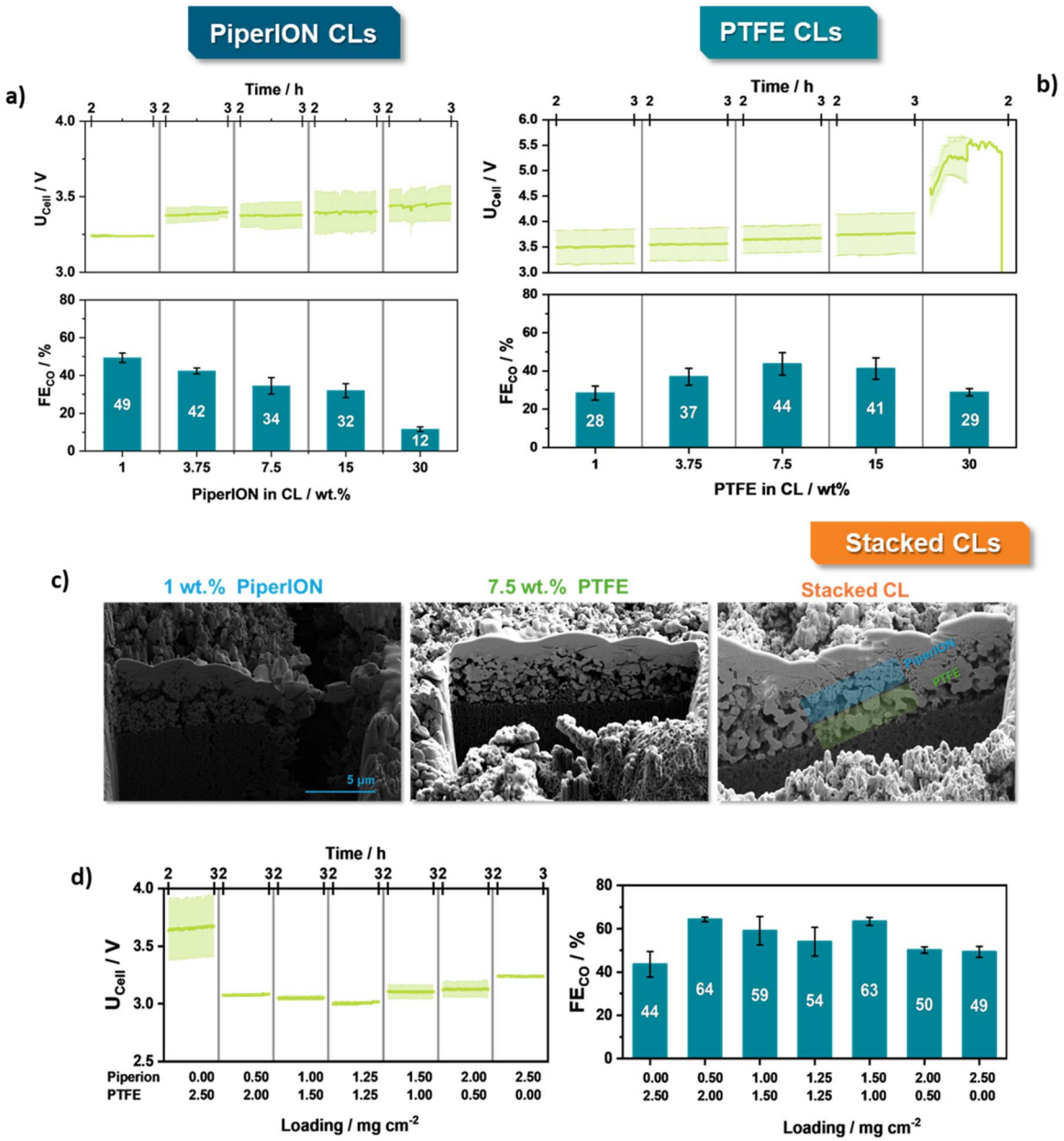

Fig. 3 Electrochemical characterization of the herein presented catalytic layers/GDEs at 300 mA cm^{-2} at 60 °C between 2nd and 3rd hour of electrolysis for the PiperION-bound CLs (a), PTFE-bound (b) and stacked (d) CLs. FIB-SEM analysis of the different catalytic layers (c).

stream has been shown to be a crucial contributor to the obtained CO_2R activity.[14,16]

Electrochemical investigation of the stacked catalytic layers

Overall, our single CL investigations show that significantly low amounts of PiperION as well as median amount of PTFE lie at the optimal performance point for the two binder types.

Taking these two optimal values, we set out to create the stacked catalytic layers. Specifically, by combining the best PTFE based CL (7.5 wt%) and the best Piperion based CL (1 wt%) a novel combined CL was fabricated and electrochemically investigated under similar conditions. Moreover, to better identify the optimal ratio between the hydrophilic/hydrophilic CLs, the overall catalyst loading of the two CLs was varied in a stepped manner. To ensure comparability of the stacked CL to the previously shown Piperion and PTFE-based CLs, the overall catalyst loading was always kept constant at 2.5 mg cm^{-2} of Ag-NPs. For example, if in a first step the PTFE-ink was applied to the GDL with a catalyst loading of 2 mg cm^{-2}, in a subsequent second step additional 0.5 mg cm^{-2} Ag-NPs were applied by spray coating the catalyst ink containing 1 wt% of PiperION. Overall, increasing the loading of an individual segment, also leads to an increase of the respective layer thickness shifting the catalytic interlayer bounds and catalytic properties of the CL Moreover, analysis *via* FIB-SEM interestingly showed that during the preparation of the stacked CLs the previously observed morphologies of the optimized CLs are fully maintained. The PTFE-layer features a microporous structure in which the Ag and PTFE particles are distinguishable, while the PiperION layer maintains its porous structure, with no clear indication of mixing of the two layers (Fig. 3c). Contact angle measurements reveal that PiperION-CLs exhibit a highly hydrophilic surface, whereas PTFE-CLs, as anticipated, display hydrophobic properties that intensify with increasing PTFE content. Interestingly, the stacked-CLs maintain a predominantly hydrophilic character due to the presence of PiperION, although contact angles close to 60° are observed in the tested configurations (Table S3†).

Overall, at 300 mA cm^{-2}, the generated stacked CLs outcompete their counterparts in every loading variation both in terms of FE_{CO} but also cell voltage. Specifically, stacked CLs featuring either a thin layer of PiperION-CL of 0.5 mg cm^{-2} or slightly higher loading of PiperION of 1.5 mg cm^{-2} show the highest CO_2R performance with a FE_{CO} of 64% at a U_{Cell} of 3.1 V. While other variations do not outcompete the distinct CLs, they overall show an improvement of the U_{Cell} value, with the equally distributed stacked-CL (1.25|1.25 mg cm^{-2}) demonstrating an improvement of 200 and 600 mV against the pure PiperION and PTFE-CL, respectively (Fig. 3d). Notably, EIS analysis revealed an important difference between the distinct CLs and the stacked variant. While both the single PTFE and PiperION-CLs feature a diffusion limited region, this is not the case for the stacked variant, for which two clear semi-circles can be seen (Fig. S5†). The overall HFR as well as charge-transfer resistance does not appear to starkly differ among identically tested GDEs. In combination with the FE_{CO} trends, this difference indicates that the combination of a hydrophobic PTFE-CL underneath the more hydrophilic PiperION-CL allows for an improved diffusion of CO_2 and water to the catalytic centres, possibly shifting the catalytic interface towards either a CO_2R ameliorating region, or improving the removal of build-up carbonates close to the catalytic layer, as we point out later on in our manuscript. Here, further in-depth investigations through a previously reported five-electrode set-up to better understand how the cell voltage distribution changes depending on the employed CL-architecture.

Moreover, to fully elucidate the necessity of Ag in the PiperION-CL we also performed controlled experiments by either spray-coating or drop-casting an ionomer layer on the PTFE-based GDE (Fig. S6†). Notably, both control variants show FE_{CO} values at *ca.* 20% after 3 h of electrolysis. These results show that the existence of Ag in the stacked architecture could be highly necessary for the elevated CO_2R performance and is only the result of better ionic conductivity within the PTFE-CL. Furthermore, maintaining a loading of 1.5 mg cm^{-2} of the PiperION-CL on the stacked layer, we also varied the amount of added PiperION in the respective CL from 1 to 30 wt%. (Fig. S7†). Here, again the 1 wt% variant shows the highest FE_{CO} values of 54%, showing how the results of our different layer optimizations are directly transferable to the stacked variant.

During long-term electrolysis at 300 mA cm^{-2}, the CO_2R ameliorating effect of the stacked CLs becomes even more evident. Setting an FE_{CO} value of 30% as the lowest limit for an acceptable performance of an investigated GDE, the CLs show different degradation behaviours depending on the employed binder, after an initial conditioning period of the GDEs and system which possibly lies between 5–10 hours of electrolysis. Notably, the more hydrophilic PiperION-based CL shows the highest degradation rate of 1.1% FE_{CO} h^{-1}, followed by the PTFE-CL at 0.8% FE_{CO} h^{-1} (Fig. 4). In both cases K-salt build up could be observed in the channels of the employed parallel flow field (Fig. S8†). In comparison, the stacked-CL reaches the 30% limit after 100 h. Notably, the previously mentioned conditioning period (5–10 h) further highlights how under optimized operational conditions,[16] such as the relative humidification, cell compression, and orientation of the cell at 60 °C, larger time amounts are required to observe the clear degradation of GDEs and CLs and observed clear differences in the performance, as shown by the similar FE_{CO} values by the PTFE and PiperION-CL during long-term testing.

Moreover, it is important to point out that whilst our CLs showed an improved performance against their counterparts, the obtained CO_2R performance must be further improved to achieved industrial relevance. Here, multiple routes can be followed to yield an improved performance, involving regeneration protocols, tailored flow-field structures, and CO_2/H_2O ratios or the use of more dissolvable Cs-salts in the anolyte as we have previously shown.[16,17] One approach we are currently exploring is the addition of carbon black in the PTFE-CL towards increasing the porosity of the PTFE-CL as well as the electrical conductivity within in, leading to an increase in FE_{CO} to 75% at a U_{Cell} of 3.0 V, with this approach requiring further exploration (Fig. S9†).

All in all, inspired by our electrolysis and EIS data, as well as post-electrolysis photographs of the flow-fields showing

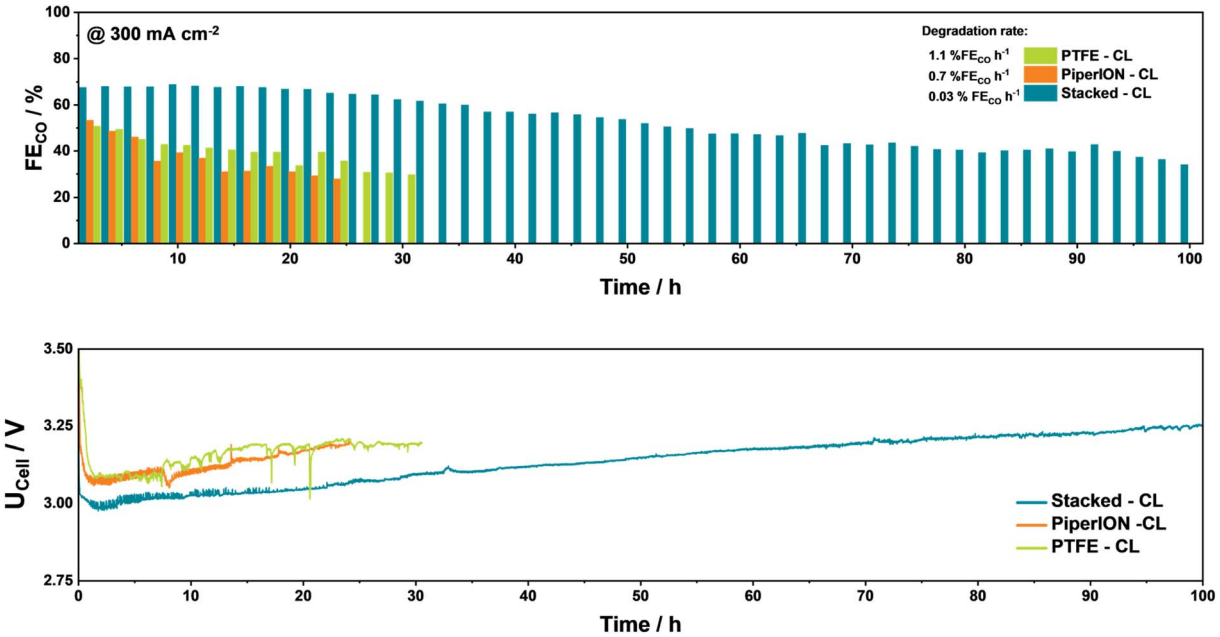

Fig. 4 Long-term investigation of the different CLs at 300 mA cm^{-2} at 60 °C with 0.1 M $KHCO_3$ as the anolyte.

carbonate accumulation after complete flooding of the various electrodes, we propose that the ability of stacked CLs to mitigate carbonate accumulation stems from their potentially enhanced pore structure and ionic conductivity. The larger pores in the PTFE-CL facilitate a more controlled accumulation of carbonate salts, which can be washed out more efficiently by the humidified stream. At the same time, the porous structure of the PiperION-CL appears crucial, not only for improving carbonate removal toward the anode from the AEM but also for directing accumulated carbonates and water to the PTFE-CL. In contrast, employing only an ionomer layer does not achieve the same effect.

Conclusions

We herein present a promising stacked CL-platform towards decoupling CO_2 reduction, ion and electron transport within the catalytic layer of zero-gap electrolysers, creating an individually tuneable GDE. Notably, under industrially applicable conditions our stacked CLs outcompete their single-binder counterparts, showing how careful design of the electrode architecture can lead both to higher selectivity and electrochemical stability. Interestingly, we show that this stacked variation is more than the sum of its parts. Similarly, we provide the community with descriptive information on the influence of the binder nature content both from an electrochemical and physical standpoint. As the results of this study show, we believe that ink engineering and rheological measurements must gain further importance as catalytic layers are tuned for novel electrocatalysts, providing an anchoring point for the creation of long-term stable and more efficient CO_2R electrolysers, going beyond Ag-based CLs and carbon-based GDLs to PTFE membranes or mesh-based ones.[18] Notably, the creation of the anchoring point cannot only be achieved through ''brute-force'' electrochemical testing but also the development of tailored *operando* cells for the CO_2R in ZGE-architecture, specifically, through *e.g.* tomography techniques, that allow for the analysis of the catalytic layer and the effects of cell compression as well as water/carbonate transport during operation.

Data availability

All data supporting the findings can be found in the article and ESI† or is available from the authors upon request.

Author contributions

Conceptualization: L. H., K. P., D. C. G., K. j. P., D. S. K. W. and U.-P. A.; methodology: L. H., K. P., D. C. G., D. B., D. S., K. j. P., K. W., and U.-P. A.; data curation: L. H., K. P., D. C. G., D. B., F. B., formal analysis: L. H., K. P., D. C. G., D. B., K. j. P.; funding acquisition: R. C., K. W. U.-P. A.; supervision: D. S., K. j. P., K. W., and U.-P. A.; writing – original draft preparation: L. H., K. P.,D. C. G., D. B., K. j. P., D. S., R. C., K. W. and U.-P. A. All authors have read and agreed to the published version of the manuscript.

Conflicts of interest

There are no conflicts to declare.

Acknowledgements

K. P. acknowledges the Fonds of the Chemical Industry for a PhD Fellowship. U.-P. A. was funded by the Deutsche Forschungsgemeinschaft (DFG, German Research Foundation)

under Germany's Excellence Strategy – EXC 2033 – 390677874 – RESOLV as well as APAP242/9-1, the Fraunhofer Internal Programs under grant no. Attract 097-602175 and ''MAT4HY-NRW'' (KP22-065-A) grant for the state NRW. Da. S. is grateful to BMBF for the financial support within the NanoMatFutur Project "H_2Organic" no. 03XP0421.

Notes and references

1 (*a*) I. E. L. Stephens, K. Chan, A. Bagger, S. W. Boettcher, J. Bonin, E. Boutin, A. K. Buckley, R. Buonsanti, E. R. Cave, X. Chang, S. W. Chee, A. H. M. Da Silva, P. de Luna, O. Einsle, B. Endrődi, M. Escudero-Escribano, J. V. Ferreira de Araujo, M. C. Figueiredo, C. Hahn, K. U. Hansen, S. Haussener, S. Hunegnaw, Z. Huo, Y. J. Hwang, C. Janáky, B. S. Jayathilake, F. Jiao, Z. P. Jovanov, P. Karimi, M. T. M. Koper, K. P. Kuhl, W. H. Lee, Z. Liang, X. Liu, S. Ma, M. Ma, H.-S. Oh, M. Robert, B. R. Cuenya, J. Rossmeisl, C. Roy, M. P. Ryan, E. H. Sargent, P. Sebastián-Pascual, B. Seger, L. Steier, P. Strasser, A. S. Varela, R. E. Vos, X. Wang, B. Xu, H. Yadegari and Y. Zhou, *J. Phys. Energy*, 2022, **4**, 42003; (*b*) P. de Luna, C. Hahn, D. Higgins, S. A. Jaffer, T. F. Jaramillo and E. H. Sargent, *Science*, 2019, 364; (*c*) O. S. Bushuyev, P. de Luna, C. T. Dinh, L. Tao, G. Saur, J. van de Lagemaat, S. O. Kelley and E. H. Sargent, *Joule*, 2018, **2**, 825; (*d*) S. Chen, C. Ye, Z. Wang, P. Li, W. Jiang, Z. Zhuang, J. Zhu, X. Zheng, S. Zaman, H. Ou, L. Lv, L. Tan, Y. Su, J. Ouyang and D. Wang, *Angew. Chem., Int. Ed.*, 2023, **62**, e202315621; (*e*) J. Zhu, J. Li, R. Lu, *et al.*, Surface passivation for highly active, selective, stable, and scalable CO_2 electroreduction, *Nat. Commun.*, 2023, **14**, 4670; (*f*) J. Liu, R. Burciaga, S. Tang, *et al.*, *Innovation Mater.*, 2024, **2**(3), 100090.

2 (*a*) P. Debergh, O. Gutiérrez-Sánchez, M. N. Khan, Y. Y. Birdja, D. Pant and M. Bulut, *ACS Energy Lett.*, 2023, **8**, 3398; (*b*) A. Raya-Imbernón, A. A. Samu, S. Barwe, G. Cusati, T. Fődi, B. M. Hepp and C. Janáky, *ACS Energy Lett.*, 2024, **9**, 288.

3 (*a*) Q. Xu, A. Xu, S. Garg, A. B. Moss, I. Chorkendorff, T. Bligaard and B. Seger, *Angew. Chem., Int. Ed.*, 2023, **62**, e202214383; (*b*) B. Siritanaratkul, M. Forster, F. Greenwell, P. K. Sharma, E. H. Yu and A. J. Cowan, *J. Am. Chem. Soc.*, 2022, **144**, 7551; (*c*) H. Shin, K. U. Hansen and F. Jiao, *Nat. Sustain.*, 2021, **4**, 911; (*d*) B. Endrődi, A. Samu, E. Kecsenovity, T. Halmágyi, D. Sebők and C. Janáky, *Nat. Energy*, 2021, **6**, 439; (*e*) B. Endrődi, E. Kecsenovity, A. Samu, T. Halmágyi, S. Rojas-Carbonell, L. Wang, Y. Yan and C. Janáky, *Energy Environ. Sci.*, 2020, **13**, 4098.

4 (*a*) J. C. Bui, C. Kim, A. J. King, O. Romiluyi, A. Kusoglu, A. Z. Weber and A. T. Bell, *Acc. Chem. Res.*, 2022, **55**, 484; (*b*) A. Böhme, J. C. Bui, A. Q. Fenwick, R. Bhide, C. N. Feltenberger, A. J. Welch, A. J. King, A. T. Bell, A. Z. Weber, S. Ardo and H. A. Atwater, *Energy Environ. Sci.*, 2023, **16**, 1783; (*c*) B. Kim, F. Hillman, M. Ariyoshi, S. Fujikawa and P. J. Kenis, *J. Power Sources*, 2016, **312**, 192.

5 U. O. Nwabara, A. D. Hernandez, D. A. Henckel, X. Chen, E. R. Cofell, M. P. de-Heer, S. Verma, A. A. Gewirth and P. J. A. Kenis, *ACS Appl. Energy Mater.*, 2021, **4**, 5175.

6 T. Jaster, S. Albers, A. Leonhard, M.-A. Kräenbring, H. Lohmann, B. Zeidler-Fandrich, F. Özcan, D. Segets and U.-P. Apfel, *J. Phys. Energy*, 2023, **5**, 24001.

7 (*a*) O. Romiluyi, N. Danilovic, A. T. Bell and A. Z. Weber, *Electrochem. Sci. Adv.*, 2023, **3**, e2100186; (*b*) Y. Chen, J. A. Wrubel, A. E. Vise, F. Intia, S. Harshberger, E. Klein, W. A. Smith, Z. Ma, T. G. Deutsch and K. C. Neyerlin, *Chem. Catal.*, 2022, **2**, 400.

8 (*a*) G. A. El-Nagar, F. Haun, S. Gupta, S. Stojkovikj and M. T. Mayer, *Nat. Commun.*, 2023, **14**, 2062; (*b*) J. Disch, L. Bohn, S. Koch, M. Schulz, Y. Han, A. Tengattini, L. Helfen, M. Breitwieser and S. Vierrath, *Nat. Commun.*, 2022, **13**, 6099.

9 (*a*) L. M. Baumgartner, A. Goryachev, C. I. Koopman, D. Franzen, B. Ellendorff, T. Turek and D. A. Vermaas, *Energy Adv.*, 2023, **2**, 1893; (*b*) K. Junge Puring, D. Siegmund, J. Timm, F. Möllenbruck, S. Schemme, R. Marschall and U.-P. Apfel, *Adv. Sustainable Syst.*, 2021, **5**, 2000088.

10 M. Sassenburg, M. Kelly, S. Subramanian, W. A. Smith and T. Burdyny, *ACS Energy Lett.*, 2023, **8**, 321.

11 (*a*) D. Siegmund, S. Metz, V. Peinecke, T. E. Warner, C. Cremers, A. Grevé, T. Smolinka, D. Segets and U.-P. Apfel, *JACS Au*, 2021, **1**, 527; (*b*) D. Segets, C. Andronescu and U.-P. Apfel, *Nat. Commun.*, 2023, **14**, 7950.

12 V. Chanda, D. Blaudszun, L. Hoof, I. Sanjuán, K. Pellumbi, K. Junge Puring, C. Andronescu and U.-P. Apfel, *ChemElectroChem*, 2024, **11**, e202300715.

13 P. Jeanty, C. Scherer, E. Magori, K. Wiesner-Fleischer, O. Hinrichsen and M. Fleischer, *J. CO2 Util.*, 2018, **24**, 454.

14 L. Hoof, N. Thissen, K. Pellumbi, K. junge Puring, D. Siegmund, A. K. Mechler and U.-P. Apfel, *Cell Rep. Phys. Sci.*, 2022, **3**, 100825.

15 K. Seteiz, J. N. Häberlein, P. A. Heizmann, L. Bohn, S. Vierrath and J. Disch, *ACS Appl. Eng. Mater.*, 2024, **2**, 1654.

16 (*a*) L. Hoof, K. Pellumbi, S. Heuser, D. Siegmund, K. junge Puring and U.-P. Apfel, *Chem. Ing. Tech.*, 2023, **95**, 668; (*b*) K. Pellumbi, D. Krisch, C. Rettenmaier, H. Awada, H. Sun, L. Song, S. A. Sanden, L. Hoof, L. Messing, K. j. Puring, D. Siegmund, B. R. Cuenya, W. Schöfberger and U.-P. Apfel, *Cell Rep. Phys. Sci.*, 2023, **4**, 101746.

17 (*a*) J. Disch, L. Bohn, L. Metzler and S. Vierrath, *J. Mater. Chem. A*, 2023, **11**, 7344; (*b*) A. B. Moss, S. Garg, M. Mirolo, C. A. Giron Rodriguez, R. Ilvonen, I. Chorkendorff, J. Drnec and B. Seger, *Joule*, 2023, **7**, 350.

18 A. H. M. da Silva, S. J. Raaijman and P. J. Corbett, *J. Chem. Eng.*, 2024, **494**, 152366.